Luminescence, CPL and magnetic properties of 1D enantiopure Ln3+ complexes with (S-) and (R-) α-methoxyphenylacetate ligand†

Ànnia Tubau,[a] Francesco Zinna,[b] Lorenzo Di Bari,[*b] Mercè Font-Bardía[c] and Ramon Vicente [*a]

[a]Departament de Química Inorgànica i Orgànica, Secció de Química Inorgànica, Universitat de Barcelona, Martí i Franquès 1-11, 08028 Barcelona, Spain. E-mail: rvicente@ub.edu

[b]Dipartimento di Chimica e Chimica Industriale, Università di Pisa, via Moruzzi 13, I 56124 Pisa, Italy. E-mail: lorenzo.dibari@unipi.it

[c]Departament de Mineralogia, Cristal lografia i Dipòsits Minerals and Unitat de Difracció de Raigs X. Centres Científics i Tecnològics de la Universitat de Barcelona (CCiTUB). Universitat de Barcelona, Solé i Sabarís 1-3, 08028 Barcelona, Spain

Abstract

The reaction of $Ln(NO_3)_2 \cdot 6H_2O$ (Ln = Eu, Tb, Dy and Sm) with (R)-(−)-α-methoxyphenylacetic acid (R-HMPA) and 1,10-phenanthroline (phen) in $EtOH/H_2O$ allows the isolation of 1D chiral compounds of formula $[Ln(\mu\text{-R-MPA})(R\text{-MPA})_2(phen)]_n$ in which Ln = Eu (R-Eu), Tb (R-Tb), Dy (R-Dy) and Sm (R-Sm). The same synthesis by using (S)-(+)-α-methoxyphenylacetic acid (S-HMPA) instead of (R)-(−)-α-methoxyphenylacetic acid allows the isolation of the enantiomeric compounds with formula $[Ln(\mu\text{-S-MPA})(S\text{-MPA})_2(phen)]_n$ where Ln = Eu (S-Eu), Tb (S-Tb), Dy (S-Dy) and Sm (S-Sm). Single crystal X-Ray diffraction measurements were performed for compounds R/S-Eu, R/S-Tb, S-Dy and S-Sm. The luminescence and the circular dichroism measured in the solid state are reported. All compounds show sensitized luminescence, notably the Eu^{3+} and Tb^{3+} ones, whose emission color can be perceived by the naked eye. For the Eu^{3+} and Tb^{3+} derivatives the quantum yield and the circular polarized luminescence have been measured. For the magnetic allowed transition $^5D_0 \rightarrow {}^7F_1$ of the Eu^{3+} compound, the anisotropy factor g_{lum} is ±0.013 (+for S-Eu). Also, magnetic properties of all compounds were studied with the Dy^{3+} analogue showing slow relaxation of the magnetization under a direct current magnetic field of 1000 Oe.

1. Introduction

Lanthanide(III) compounds are currently mainly studied for their peculiar magnetic and luminescent properties derived from their partially filled 4f valence shell. Regarding magnetic properties, since the discovery of the first mononuclear lanthanide complexes of formula $[Pc_2Ln]^- \cdot TBA^+$ (Ln = Tb, Dy; Pc = dianion of phthalocyanine; TBA^+ = tetrabutylammonium) showing slow magnetization relaxation and acting as single molecule magnets (SMMs),[1] a plethora of mono and polynuclear SMMs complexes derived from lanthanide ions with large orbital momentum and strong magnetic anisotropy have been reported.[2] On the other hand, lanthanide(III) complexes with luminescence properties are of interest due to their applications in materials and biosciences.[3] The preparation of chiral lanthanide(III) coordination compounds is of high current interest to achieve circularly polarized luminescence (CPL)[4] for applications in circularly polarized organic lightemitting diodes (CP-OLEDs),[5] biological sensing[6] and anticounterfeiting devices.[7] Moreover, CPL active lanthanide complexes are studied in the context of molecular magnetism.[8] The chiral ligands naturally induce a dissymmetric environment around the Ln^{3+} ion, which determines the onset of chiroptical properties allied to the f–f transitions of the ion. In emission this is sensitively monitored through CPL, which can be conveniently quantified by means of the dissymmetry factor g_{lum}, eqn (1):

$$g_{lum} = 2\,\frac{I_L - I_R}{I_L + I_R} = 2\,\frac{\Delta I}{I} \tag{1}$$

where I_L and I_R are the left and right circularly polarized components of the emission of the compound.

Usually, non-aggregated organic molecules or d-metal complexes display g_{lum} factors of the order of 10^{-4}–10^{-3},[9] while lanthanide complexes may show much higher values (10^{-1}– 1.4).[10] Usually, CPL is measured for mononuclear Eu^{3+} complexes, while it

81 is more rarely investigated for complexes with higher nuclearity, such as binuclear

82 helicates[11] or trinuclear[12] and heptanuclear[13] systems.

83 Recently[14] we have used the chiral bidentate bridging carboxylate ligands generated

84 from (S)-(+)- or (R)-(−)-2-phenylpropionic acid and S-(+)- and R-(−)-2-(6-methoxy-2-

85 naphthyl)propionic acid to synthesize two series of enantiomeric pure dinuclear 4f-metal ion

86 complexes of formula $[Ln_2(SL)_6(phen)_2]$ or $[Ln_2(R-L)_6(phen)_2]$ (HL = chiral carboxylic

87 acid) by adding simultaneously neutral chelating 1,10-phenanthroline (phen) ligands which

88 block two coordination sites per Ln^{3+} ion and terminate further aggregation. The 1,10-

89 phenanthroline ligands have also the role to sensitize the luminescence of the lanthanide ion,

90 through the so-called antenna effect. In fact, because of the weak f–f absorption of trivalent

91 lanthanide ions, a suitable chromophoric organic ligand should be employed to populate the

92 lanthanide emitting states through an energy transfer process.[15]

93 For the published R and S complexes of formula $[Eu_2(2\text{-phenylpropionate})_6(phen)_2]$

94 and $[Eu_2([2\text{-}(6\text{-methoxy-2-naphthyl}) propionate])_6(phen)_2]$, the analysis of the data yielded

95 values of g_{lum} factors for $^5D_0 \rightarrow {^7F_1}/{^7F_2}$ transitions around $g_{lum} = \pm 1 \times 10^{-2}$ and $g_{lum} =$

96 $\pm 1 \times 10^{-3}$ respectively.[14]

97 With the aim to obtain new lanthanide compounds in which luminescent, chiroptical

98 and magnetic properties could coexist, and therefore, obtain multifunctional materials, we

99 present herein the structural, magnetic and optical studies of eight new chiral lanthanide

100 coordination complexes derived from the use of the pure enantiomeric R- or S-species of the

101 α-methoxyphenylacetic acid (R- and S-HMPA respectively, (Scheme 1)) and the auxiliary

102 ligand 1,10-phenanthroline. The reaction of the above ligands with the respective nitrate

103 lanthanide salts lead to new 1D complexes with the formula $[Ln(\mu\text{-R-MPA})(R\text{-}$

104 $MPA)_2(phen)]_n$ or $[Ln(\mu\text{-S-MPA})(SMPA)_2(phen)]_n$ for R- or S-HMPA respectively (Ln =

105 Eu, Tb, Dy and Sm). The presence of the methoxy group in the α-methoxyphenylacetate

106 ligand induces the formation of a 1D polymeric chain along the a axis instead of the dinuclear

107 compounds of formula $[Ln_2(R/S-L)_6(phen)_2]$ found for the previous chiral compounds

108 published by our group where R/S-L = R/S-2-phenylpropionic acid and R/S-2-(6-methoxy-

109 2-naphthyl)propionic acid.[14]

2. Experimental section

Starting materials

Ln(NO$_3$)$_3$·6H$_2$O salts, (S)-(+)- or (R)-(−)-α-methoxyphenylacetic acid and 1,10-phenantroline (Aldrich) were used as received.

Synthesis of 1D complexes [Ln(μ-R/S-MPA)(R/S-MPA)$_2$(phen)]$_n$.

Into 20 mL of an ethanol/water solution in the 1 : 1 ratio, the respective R/S-α-methoxyphenilacetic acid (1.5 mmol, 249 mg) and KOH (1.5 mmol, 84.2 mg) were dissolved. Then, 1,10-phenantroline (0.3 mmol, 54 mg) dissolved in 5 mL of ethanol/water (1 : 1) was added. Afterward, a solution (5 mL) in the same ethanol/water ratio with the Ln(NO$_3$)$_3$·nH$_2$O salt (0.22 mmol) was added dropwise into the reaction mixture. The colorless solution was magnetically stirred for 1 h and then left to stand at room temperature. After 1 week, needle shaped white single crystals suitable for monocrystal X-Ray diffraction appeared. Anal. Calc. (%) for R-Eu C, 56.6; H, 4.3; N, 3.4, found: C, 57,0; H, 4.4; N, 3.4. Calc(%) for S-Eu C, 56.6; H, 4.3; N, 3.4, found: C, 56.6; H, 4.6; N, 3.4. Calc. (%) for R-Tb C, 56.1; H, 4.2; N, 3.4, found: C, 56.5; H, 4.4; N, 3.4. Calc(%) for S-Tb C, 56.1; H, 4.2; N, 3.4, found: C, 56.2; H, 4.3; N, 3.4. Calc. (%) for R-Sm C, 56.7; H, 4.3; N, 3.4, found: C, 57,0; H, 4.3; N, 3.4. Calc(%) for S-Sm C, 56.7; H, 4.3; N, 3.4, found: C, 56.5; H, 4.4; N, 3.4. Calc. (%) for R-Dy C, 55.9; H, 4.2; N, 3.3, found: C, 56.2; H, 4.2; N, 3.3. Calc(%) for S-Dy C, 55.9; H, 4.2; N, 3.3, found: C, 56.2; H, 4.2; N, 3.3. Selected IR bands (KBr pellet, cm−1, Fig. S1†) 3083–2817 (w), 1608 (m), 1552 (s), 1509 (m), 1400 (s), 1326 (w), 1196 (m), 1100 (m), 1065 (m), 987 (m), 839 (m), 713 (s, split), 635(m) for R-Eu, 3086–2817 (w), 1613 (m), 1557 (s), 1509 (m), 1404 (s), 1317 (w), 1200 (m), 1096 (m), 1065 (m), 983 (m), 839 (m), 713 (s, split), 635 (m) for S-Eu, 3091–2817 (w), 1613 (m), 1561 (s), 1509 (m), 1404 (s), 1330 (w), 1200 (m), 1096 (m), 1070 (m), 983 (m), 839 (m), 717 (s, split), 635 (m) for R-Tb, 3091–2817 (w), 1613 (m), 1557 (s), 1509 (m), 1404 (s), 1330 (w), 1200 (m), 114 (m), 1065 (m), 991 (m), 839 (m), 717 (s, split), 635 (m) for S-Tb, 3091–2817 (w), 1609 (m), 1552 (s), 1509 (m), 1396 (s), 1326 (w), 1200 (m), 1100 (m), 165 (m), 983 (m), 843 (m), 713 (s, split), 635 (m) for R-Sm, 3091–2813 (w), 1609 (m), 1574 (s), 1509 (m), 1396 (s), 1322 (w), 1196 (m), 1104 (m), 1065 (m), 991 (m), 839 (m), 713 (s, split), 635 (m) for S-Sm, 3087–2817 (w), 1617 (m), 1569 (s), 1513 (m), 1396 (s), 1326 (w), 1204 (m), 1096 (m), 1065 (m), 983 (m), 839 (m), 717 (s, split), 635 (m) for R-Dy and 3087–2817 (w), 1617 (m), 1569 (s), 1513 (m), 1396 (s), 1326 (w), 1204 (m), 1096 (m), 1065 (m), 983 (m), 839 (m), 717 (s, split), 635 (m) for S-Dy.

IR and magnetic measurements

Infrared spectra (4000–400 cm^{-1}) were recorded from KBr pellets on a PerkinElmer 380-B spectrophotometer.

Magnetic measurements were performed on solid polycrystalline samples with a Quantum Design MPMS-XL SQUID magnetometer at the Magnetic Measurements Unit of the University of Barcelona. Pascal's constants were used to estimate the diamagnetic corrections, which were subtracted from the experimental susceptibilities to give the corrected molar magnetic susceptibilities.

Luminescence properties

Solid state fluorescence spectra of compounds were recorded on a Horiba Jobin Yvon SPEX Nanolog fluorescence spectrophotometer (Fluorolog-3 v3.2, HORIBA Jobin Yvon, Cedex, France) equipped with a three slit double grating excitation and emission monochromator with dispersions of 2.1 nm mm^{-1} (1200 grooves per mm) at room temperature. The steady-state luminescence was excited by unpolarized light from a 450 W xenon CW lamp and detected at an angle of 22.5° for solid state measurement by a red-sensitive Hamamatsu R928 photomultiplier tube. The equipment was adjusted to obtain the highest background-to-noise ratio. Spectra were corrected for both the excitation source light intensity variation (lamp and grating) and the emission spectral response (detector and grating).

The excited state decay curves were measured in the same instrument in the phosphorescence mode using a 450 W xenon pulsed lamp (λ = 371 nm, 1.5 ns pulse). The measured decays were analyzed using the Origin software package. Both decay curves fitted monoexponentially:

$I(t) = I_0 \left(-\frac{t}{\tau_{obs.}} \right)$ The fit quality was determined by the χ^2 method of Pearson. Absolute quantum yield (Φ_{TOT}) measurements were acquired in the G8 Quantum Integrating Sphere from GMP with an interior reflective coating made of Spectralon®. Then the Φ_{TOT} was calculated following eqn (2):

$$\Phi = \frac{E_c - E_c \ (blank)}{L_a - L_c} \tag{2}$$

L_a is the calculated area of the outgoing amount of light

172   without interaction with a sample (blank) at the used λ_{exc} and L_c after interaction with the

173   sample. E_c refers to the calculated area from the emission spectrum of the sample and E_c (blank)

174   from the emission spectrum of the blank. Band pass of 0.3 nm for the QY measurements and of 0.5

175   nm for lifetime measurements were employed in order to not surpass the 10^6 CPS to make sure that

176   we are not measuring in the non-linear optic zone, otherwise the results would not be correct.

177

Chiroptical spectroscopy measurements

179   **ECD spectra.** ECD spectra were recorded with a Jasco J-1500 spectropolarimeter on the

180   polycrystalline samples dispersed in a KBr matrix. In order to check for and minimize contributions

181   from linear dichroism/linear birefringence, for each sample, different spectra were recorded rotating

182   the sample by 180° around the optical axis and then all the spectra were averaged.

183   **CPL spectra.** The circularly polarized luminescence experiments for compounds S/R-Eu

184   and S/R-Tb were carried out with a home-built CPL spectrofluoropolarimeter[16] that acquires

185   simultaneously the luminescence and CPL data, under UV irradiation (λ_{max} = 254 nm) on quartz

186   plate depositions. The depositions of the complexes were obtained from n-pentane dispersions. N-

187   pentane was chosen as a dispersant as it does not dissolve the compounds and in this way the

188   complexes are deposited as a microcrystalline powder film. Several spectra were acquired rotating

189   the sample by ±45° around the optical axis and by flipping the sample by 180° around the axis

190   perpendicular to the collection beam.

191   **X-ray crystallography.** Good quality crystals of R/S-Eu, R/S-Tb, S-Dy and S-Sm were

192   selected and mounted on a D8VENTURE (Bruker) diffractometer with CMOS detector. The

193   crystallographic data, conditions retained for the intensity data collection, and some features of the

194   structure refinements are listed in Table S1.† All the structures were refined by the least-squares

195   method. Intensities were collected with a multilayer monochromated Mo-Kα radiation. Lorentz

196   polarization and absorption corrections were made for the R/S-Eu, R/S-Tb, S-Dy and S-Sm crystal

197   measurements. The structures were solved by direct methods, using the SHELXS-97 computer

198   program[17] and refined by full-matrix least-squares method, using the SHELXL-2014 computer

199   program.[18] The non-hydrogen atoms were located in successive difference Fourier syntheses and

200   refined with anisotropic thermal parameters on F^2. For hydrogen atoms isotropic temperature factors

201   have been assigned as 1.2 respective of the C atom in which the H is attached.

202

3. Results and discussion

General syntheses

A straightforward room temperature synthetic route using the R/S-α-methoxyphenylacetic acid (HMPA), 1,10-phenantroline (phen) and $Ln(NO_3)_3 \cdot H_2O$ (Ln = Eu R/S-Eu, Tb R/S-Tb, Dy R/S-Dy and Sm R/S-Sm) with further slow evaporation of the solvent, lead to enantiopure chiral R/S-$[Ln(\mu\text{-MPA})(MPA)_2(phen)]_n$ 1D chain compounds. Several trials were carried out before concluding that the best conditions for obtaining single crystals suitable for monocrystal X-Ray diffraction were by using an excess of the R/S-HMPA ligand with H2O/EtOH in a 1 : 1 (v/v) proportion as the solvent.

Molecular structures of the R/S-$[Ln(\mu\text{-MPA})(MPA)_2(phen)]_n$ compounds. Single crystal X-Ray diffraction measurements were performed for compounds R/S-Eu, R/S-Tb, S-Dy and S-Sm. All the compounds crystallize in the monoclinic $P2_1$ space group. The asymmetric unit of R/S-Ln consists of a unit formed by one Ln^{3+} ion, two chelating R/S-α-methoxyphenylacetate (R/S-MPA) ligands, one R/S-MPA bridging ligand and one phen molecule. The asymmetric unit is expanded in space forming a 1D polymeric chain along the crystallographic a axis.

All the Ln^{3+} compounds are isostructural as it is seen in the powder X-Ray diffraction spectra (Fig. S2†), also, affirming the pure phase and crystallinity of the compounds. Therefore, only the new compound R-Eu will be discussed.

A partially labelled plot of the structure of compound R-Eu is shown in Fig. 1 and the mirror image of R/S-Eu compounds is depicted in Fig. 2. Selected bond distances of R/S-Eu, R/S-Tb, S-Dy and S-Sm and crystallographic information are listed in Table 1 and Table S1† respectively.

The structure consists of a polymeric 1D chain of formula $[Eu(\mu\text{-R-MPA})(R\text{-MPA})_2(phen)]_n$ where each Eu^{3+} is nonacoordinated. The polymeric chain extends along the [1 0 0] direction. The EuO_7N_2 coordination sphere encompasses two R-MPA ligands that are coordinated in the bidentate carboxylate chelating coordination mode (Scheme 2a) to Eu1 by the O1, O2 and O7, O8 atoms, with Eu–O distances in the range of 2.450–2.500 Å. Another R-MPA ligand is bridging two Eu^{3+} through the O7 and O8 atoms from the carboxylate group in the syn-anti conformation (Scheme 2b). The O9 oxygen atom from the methoxy group of this R-MPA ligand coordinates also to the neighbouring europium atom. The Eu–O7, Eu–O8 and Eu–O9 distances are 2.396, 2.388 and 2.539 Å respectively.

Finally, the coordination sphere of the lanthanide ion is completed by two N atoms (N1 and N2) from the 1,10-phenantroline molecule in the chelating coordination mode with Eu–N distances of 2.569

8

234   and 2.558 Å for Eu–N1 and Eu–N2 respectively. The Eu1···Eu1_a intrachain distance is 6.048 Å and

235   the shortest interchain distance is 12.298 Å. The crystal structure of S-Eu is very similar to R-Eu but

236   its configuration is mirror symmetrical with R-Eu. Symmetry operators for generating equivalent

237   positions are: (a) $-1 + x$, y, z.

238   The SHAPE software,[19] was used to determine the degree of distortion of the coordination

239   polyhedron in compound R-Eu. It consists of a distorted polyhedron between the spherical tricapped

240   trigonal prism (D_{3h}), spherical capped square antiprism (C_{4v}) and muffing (C_s) geometries with

241   Continuous Shape measurements (CShM) of 1.821, 2.084 and 2.075 respectively (Fig. 1, right). The

242   degree of distortion of the coordination geometry of the other compounds is shown in Table S2.†

243   The Ln–O and Ln–N bond lengths diminish following $Sm^{3+} > Eu^{3+} > Tb^{3+} > Dy^{3+}$,

244   confirming the lanthanide(III) contraction tendency along the 6th period.[20]

245

246   **Luminescence properties**

247   Luminescence properties of all compounds were studied and measured in the solid state at

248   room temperature. Since each enantiomer pair shows the same luminescence properties, only the R-

249   enantiomer of each lanthanide is discussed in this section. The excitation and absorbance spectra

250   measured in the solid state of the enantiomers of each compound are displayed in Fig. S3 and S4.†

251   Excitation spectra were recorded at the emission wavelength (λ_{em}) of 614 nm ($^5D_0 \rightarrow {}^7F_2$)

252   for R-Eu, at 546 nm ($^5D_4 \rightarrow {}^7F_5$) for R-Tb, at 572 nm ($^4F_{9/2} \rightarrow {}^6H_{13/2}$) for R-Dy and at 644 nm

253   ($^4G_{5/2} \rightarrow {}^6H_{9/2}$) for R-Sm. The four spectra show an intense and broad band around 300 to 360 nm

254   corresponding to the $\pi \rightarrow \pi^*$ and $n \rightarrow \pi^*$ ligand centred excitation transitions from the R-MPA and

255   phen ligands. Only for compound R-Eu, excitation arising from Eu f–f transitions could be discerned

256   at 375, 395 and 464 nm corresponding to $^5D_4 \rightarrow {}^7F_0$, $^5L_6 \rightarrow {}^7F_0$ and $^5D_2 \rightarrow {}^7F_0$ respectively. Room

257   temperature emission spectra of R-Eu, Tb, Dy and Sm, were obtained by employing an excitation

258   wavelength (λ_{exc}) of 330 nm.

259   In the emission spectra of R-Eu, (Fig. 3a) different bands can be observed at 580, 595, 614,

260   650 and 691 nm corresponding to the $^5D_0 \rightarrow {}^7F_{J = 0–4}$ transitions. $^5D_0 \rightarrow {}^7F_0$ corresponds to a

261   forbidden transition ($\Delta J = 0$), therefore its intensity is very low and in this case is almost

262   imperceptible. The magnetically allowed $^5D_0 \rightarrow {}^7F_1$ transition, with intensity independent of the

263   environment, is split due to the crystal field. For a coordination geometry with symmetry lower than

264 cubic, hexagonal, trigonal and tetragonal (meaning D_{2h}, D_2, C_{2v}, C_{2h}, C_2, C_s, S_2 or C_1), the

265 degeneracy is lifted up to $2J + 1$ m_j components due to crystal field splitting. For the $^7F_1$ state, m_j

266 values are $2J + 1 = 3$ and for the presented Eu^{3+} compound, all the three components can be discerned

267 in the emission spectra. This result is consistent with the structural characterization of R-Eu since the

268 calculated ideal coordination polyhedron with less distortion with respect to the experimental,

269 presents a distortion between the D_{3h}, C_{4v} but also with the low symmetry C_s point group.

270 Furthermore, $^5D_0 \rightarrow {}^7F_2$ is the most intense band located in the red range and responsible for the

271 red-orange emission colour that could be seen by the naked eye for S-Eu, Fig. S5.† This band is a

272 hypersensitive transition, and in the case of S-Eu, its splitting indicates that the lanthanide ion is not

273 occupying an inversion symmetry site inside the structure.[21]

274   The R-Tb compound shows green emission that could be seen by the naked eye (Fig. S5†).

275 The bands arising from the f–f Tb^{3+} transitions can be differentiated at 491, 546, 585 and 623 nm

276 corresponding to the $^5D4 \rightarrow {}^7F_{J = 6-3}$ transitions (Fig. 3b).

277   In the visible range, the bands arising from the R-Dy compounds can be observed at 481 nm,

278 corresponding to the magnetically allowed $^4F_{9/2} \rightarrow {}^6H_{15/2}$ transition, at 572 nm, corresponding to

279 the $^4F_{9/2} \rightarrow {}^6H_{13/2}$ transition and at 659 nm (weak band) corresponding to the $^4F_{9/2} \rightarrow {}^6H_{11/2}$

280 transition. Furthermore, in the near infrared (NIR) range, two bands can be observed at 996 and 1144

281 nm (Fig. S6†), which are assigned to the transitions from the $^4F_{9/2}$ energy level to $^6F_{7/2}$ and $^6F_{5/2}$

282 respectively.

283   For the R-Sm compound, four bands are identified at 563, 600, 644 and 705 nm in the visible

284 range and assigned to the $^4G_{5/2} \rightarrow {}^6H_{5/2-11/2}$ transitions (Fig. 3b), furthermore, in the NIR range, the

285 $^4G_{5/2} \rightarrow {}^6H_{15/2}$ transition can be seen as a shoulder at 896 nm. The f–f emission transitions arising

286 from the $^4G_{5/2}$ emitting level to the $^6F_{5/2-9/2}$ energy states are found at 940, 1016 and 1166 nm

287 respectively (Fig. S7†).[3a,20]

288   The excitation at the ligand absorption wavelengths for all compounds induced the expected

289 emission bands corresponding to the characteristic f–f transitions from each lanthanide ion. Also,

290 below 450 nm, no emission from the ligands is detected, indicating that energy transfer from the

291 excited states of the organic moieties to the emitting energy level of the respective lanthanide (the

292 antenna effect) takes place for these compounds.[20] Nonetheless, the overall quantum yield (ϕ^L_{Ln}),

293 that is the ratio of the photons emitted by the lanthanide to the photons absorbed by the ligand, was

294 measured with an integrating sphere with the intention to better understand the luminescent

efficiency of the presented compounds. For S-Eu the absolute quantum yield resulted to be 0.14. The photoluminescence time decay was recorded at the λ_{ex} of 330 nm and collecting the measurement at 614 nm, corresponding to the $^5D_0 \rightarrow {}^7F_2$ transition. The curve of the intensity against time (ms), showed in Fig. 3c, was fitted using a mono-exponential equation (see Experimental section) with a decay time (τ_{obs}) of 1.77 ms for the Eu^{3+} compound, confirming that the red emission of S-Eu comes from a single emitting centre and a single radiative deactivation process. In addition, more information about the sensitization mechanism that takes place for this system can be determined for the Eu^{3+} compound. The sensitization efficiency (η_{sens}) accounts to the percentage of energy absorbed by the chromophore ligands transferred to the excited state of the lanthanide ion and it is an important factor in the overall quantum yield that can be defined as: $\phi_{Ln}^L = \eta_{sens} \cdot \phi_{Ln}^{Ln}$. The other step that elucidates the ϕ_{Ln}^L is the intrinsic quantum yield (ϕ_{Ln}^{Ln}) that refers to the quantum yield once the emitting level of the Ln^{3+} ion is populated. The intrinsic quantum yield is described as the ratio between the measured time decay and the radiative lifetime $\phi_{Ln}^L = \frac{\kappa_{rad}}{\kappa_{rad} + \kappa_{non-rad}} = \frac{\tau_{obs}}{\tau_{rad}}$. Due to the pure magnetic dipole character of the $^5D_0 \rightarrow {}^7F_1$ transition, a simplified equation can be used to calculate the τ_{rad} from Eu^{3+} $^5D_0$ excited state, corresponding to the lifetime in absence of non-radiative deactivations (eqn (S1)†).[21] For S-Eu, τ_{rad} is 3.05 ms. Therefore, the ϕ_{Ln}^{Ln} is 0.58. As expected, it is higher than the measured ϕ_{Ln}^L, because the intrinsic quantum yield do not depend on the efficiency of the ligand to Ln energy transfer, however, it takes into account deactivation mechanisms such as back-transfer energy or other quenching effects. Finally, the calculated η_{sens} results of 0.24 evidencing a sensitization effect that is rather low, nevertheless it is enough for S-Eu to present the desired optical properties.[21,22]

On the other hand, the measured ϕ_{Ln}^L for the S-Tb sample was higher than the Eu^{3+} analogue, yielding 0.33. Moreover, the luminescence lifetime was measured by monitoring the emission decay at 546 nm, corresponding to the more intense emission band $^5D_4 \rightarrow {}^7F_5$, Fig. 3c. The τ_{obs} calculated from the monoexponential fitting is 1.50 ms, confirming also the presence of one type of emitting specie and emission mechanism.

For R-Dy and R-Sm, the QY and the luminescent time decay were not measured due to the low emission intensity of the compounds.

Circular dichroism (CD) and circular polarized luminescence

(CPL) measurements. The Circular Dichroism (CD) measurements were carried out in solid state on pellets containing the sample dispersed in a KBr matrix. The complexes show rather weak Cotton effects (Fig. 4). The bands around 200–460 nm are assigned mainly to the absorption of the phen ligand, with contributions from the $\pi \to \pi^*$ transition of MPA. Spectra of the free ligand are found in Fig. S8.† For these 1D lanthanide chains the ligand arrangement formed by the MPA and phen ligands are organized in the space around the metal ion conferring low dissymmetry to the complex and leading to the weak CD associated to the ligand-centered electronic transitions.

Circular Polarized Luminescence (CPL) measurements were performed for R/S-Eu and R/S-Tb. The samples were deposited in a quartz plate, from a suspension in n-pentane, which acts only as a dispersing agent, considering that the compounds are not soluble in this solvent. The emission spectra recorded simultaneously with CPL spectra were not significantly different from those measured on the polycrystalline samples (see above). This suggests that n-pentane does not induce any change to the complexes (Fig. S9†). The CPL spectra of compounds R/S-Eu recorded at the excitation wavelength of 254 nm are depicted in Fig. 3a, bottom. The Eu^{3+} enantiomeric pairs show low intensity CPL signal, nevertheless, the mirror image bands corresponding to $^5D_0 \to {}^7F_1$, $^7F_2$ and $^7F_4$ Eu(III) f–f transitions can be clearly discerned. The magnetic dipole transition, $^5D_0 \to {}^7F_1$, at 595 nm is the most intense one. Two well resolved components due to crystal field can be observed. The m_j component located in the higher energy region of the transition shows a splitting that appears as a bifid structure revealing the three crystal field splitting components. Next, at 614 nm the $^5D_0 \to {}^7F_2$ transition shows lower intensity and only one component is well differentiated. Finally, at 691 nm, the $^5D_0 \to {}^7F_4$ transition appears with very low intensity, though at least two mj components can be differentiated. The dissymmetry factor could be quantified (Eq.1) for the $^5D_0 \to {}^7F_1$ and $^5D_0 \to {}^7F_2$ transitions leading to a glum = ΔI/I of ±0.013 (+for S-Eu) for the $^5D_0 \to {}^7F_1$ transition and ±0.003 (+for the R-Eu enantiomer) for the hypersensitive transition (Table 2). The presented g_{lum} values are similar to other reported Eu^{3+} coordination compounds with carboxylate ligands and to other Eu^{3+} polymeric chain complexes measured in the solid state.[14,23] CPL measurements were performed for the S/R-Tb compounds as well, but the intensity of the obtained spectra is too low to extract meaningful information (Fig. S10†). CPL studies in polymeric Lanthanide chains and measured in the solid state remains rare.[24] Y. Hasegawa et al.[25] presented a polymeric chain complex with g_{lum} values for the magnetic dipole transition up to 0.17 measured in the solid state.

Due to low luminescence, the CPL of R/S-Dy and R/S-Sm could not be measured.

Magnetic properties

DC magnetic susceptibility studies. Since S- and R-enantiomers are expected to show the same magnetic properties, direct current (dc) magnetic susceptibility (χ_M) and magnetization (M) measurements were performed for the S-enantiomers on the polycrystalline samples. The χ_M measurements were carried out under a dc field of 0.3 T in the 2–300 K temperature range. The $\chi_M T$ dependence with T plots are presented in Fig. 5. At room temperature (300 K) the $\chi_M T$ values are 1.43, 11.41, 13.82 and 0.40 $cm^3\ mol^{-1}$ K for S-Eu, S-Tb, S-Dy and S-Sm respectively. For one isolated Ln^{3+} cation, the calculated $\chi_M T$ values are: 0 $cm^3\ mol^{-1}$ K for Eu^{3+} ground state $^7F_0$; 11.82 $cm^3\ mol^{-1}$ K for Tb^{3+} ground state $^7F_6$ and $g_j = 3/2$; 14.17 $cm^3\ mol^{-1}$ K for Dy^{3+} ground state $^6H_{15/2}$ and $g_j = 4/3$, 0.09 $cm^3\ mol^{-1}$ K for Sm^{3+} ground state $^6H_{5/2}$ and $g_j = 2/7$.[3a]

The experimental $\chi_M T$ value at room temperature for compound S-Eu is higher than 0. Due to the rather small spin–orbit coupling parameter (λ) between the $^7F_{(0-1)}$ states, at room temperature the higher energy ^7F_J states closer to the ground state are thermally populated (mainly the $^7F_1$ state). Then the $\chi_M T$ values decrease gradually on cooling the sample due to the thermal depopulation of the ^7F_J excited states. At 2 K, $\chi_M T$ is 0.017 $cm^3\ mol^{-1}$ K confirming that at low temperature the non-magnetic ground state ($J = 0$) is stabilized. The χ_M vs. T plot for compound S-Eu (Fig. S11†) shows an increase of the χ_M values when approaching to 2 K due to remnant paramagnetic rare earth impurities. If we consider the presented polymeric chain formed by non-magnetically coupled Eu^{3+} ions, the λ value can be calculated from $\chi_M T$ vs. T data considering Eu^{3+} as a free ion by using eqn (S2)†[26,27] (the plot of the $\chi_M T$ vs. T data only for S-Eu is shown in Fig. S12†). From the best fitting the λ value is 335 cm^{-1}. From the spectroscopic data, the energy gap between the $^7F_0$ and $^7F_1$ should correspond to the λ parameter. The λ value has been calculated from the emission spectra of S-Eu measured at 77 K, Fig. S13 and Table S3.† This value is 377 cm^{-1} for S-Eu. This result is similar to other Europium compounds.[28,29]

On cooling the samples, for S-Tb and S-Dy, the $\chi_M T$ values remain almost constant till ~50 K and below this temperature, the susceptibility values decrease up to 7.80 $cm^3\ mol^{-1}$ K for S-Tb and to 8.49 $cm^3\ mol^{-1}$ K for S-Dy due to thermal depopulation of the m_j states. The possibility of magnetic coupling between the Ln^{3+} ions has not been considered for these compounds due to: (i) the well shielded nature of electrons in the $4f^n$ orbitals (ii) the Ln–Ln intra and inter-molecular shortest distances are too long (6.04 ± 0.01 and 12.32 ± 0.02 Å respectively).

387   For the S-Sm compound, the $\chi_M T$ value at room temperature is also higher than the one

388 calculated for a free ion. For a Sm^{3+} ion, the ^6H ground state is split due to spin–orbit coupling by

389 $^6H_{J = 5/2-15/2}$ with a λ parameter around 200 cm^{-1}. Therefore, at room temperature, the excited ^6H_J

390 states are thermally populated. The diminution of $\chi_M T$ on cooling the sample is due to the thermal

391 depopulation of the J states.[26,27] S-Sm magnetic data could not be fitted successfully under the free

392 ion approximation.

393   Magnetization dependence with an applied magnetic field at 2 K for all compounds are

394 depicted in Fig. S14.† None of the presented compounds show saturation of the magnetization.

395

AC magnetic susceptibility studies

397   In order to study the dynamic magnetic properties of the R/S-[Ln(μ-MPA)(MPA)$_2$(phen)]$_n$

398 compounds, ac magnetic susceptibility measurements in a 4×10^{-4} T oscillating field were recorded

399 for compounds S-Tb, S-Dy and S-Sm.

400   At a 0 Oe dc external magnetic field, the in-face (χ'_M) and out-of-face (χ''_M) magnetic

401 susceptibility components were measured in an oscillating field at 10 and 1000 Hz and in the 2 to 12

402 K temperature range. Only for compound S-Dy, a temperature dependence for the χ'_M component

403 was observed, where it increases on decreasing the temperature without reaching a maximum point

404 above 2 K. Nevertheless, no χ''_M dependence with temperature and frequency was observed at all,

405 Fig. S15.† This fact suggests that the relaxation of the magnetization goes through a shortcut path

406 between the two bistable $\pm m_j$ states, the so called quantum tunneling of the magnetization (QTM).

407 In order to suppress the fast QTM, two different dc fields (10 and 1000 Oe) at different temperatures

408 where applied to the samples. Then, maxima in the χ'_M and χ''_M components were discerned below

409 8 K only for the S-Dy compound. In order to establish the optimum dc magnetic field, measurements

410 of the χ'_M and χ''_M with frequency, at a constant temperature of 3 K, and applying dc fields from 0

411 to 3000 Oe, were performed for S-Dy. A plot of τ ($1/2\pi\omega$) with the dc field shows that the relaxation

412 time is the greatest when the applied external magnetic field is 1000 Oe. Then this dc field is chosen

413 as the optimal one (Fig. S16†).

414   On performing the measurements with a 1000 Oe dc field, a dependence of the χ''_M with

415 temperature and frequencies is clearly observed and maximum points are discerned for the magnetic

416 susceptibility components below 8 K (Fig. 6, left). Nevertheless, at 2 K in the $\chi''_M(T)$ plot, a second

417 maximum is perceived suggesting a faster relaxation process differentiated from the one occurring

418 at higher temperatures (Fig. S17†). This faster mechanism probably accounts for the QTM, which is

419 not totally removed on applying the external dc field.[30]

420   The representation of the ac data in the Cole–Cole plots, Fig. 6, middle, shows semicircles

421 that are not perfectly symmetric. Furthermore, a shoulder can be discerned corresponding to the χ'_M

422 vs. χ''_M points obtained at lower temperatures and lower frequencies accounting to the faster

423 mechanism differentiated in the $\chi''_M(T)$ plot. The fit was not successful using a two component

424 generalized Debye model because of the lack of a sufficient number of experimental data points

425 corresponding to the faster mechanism. Nevertheless, a good fit was obtained for the slower process

426 using the one-component generalized Debye model (eqn (S3) and Table S4†).[31] The fitting of the

427 Cole–Cole curves were obtained using the CCFit software.[32] The representation of $\ln(\tau)$ vs. $1/T$ is

428 depicted in Fig. 6, right. The linear trend in the slope in the low temperature region was fitted by an

429 Arrhenius law. This model describes the relaxation of the magnetization by the thermally assisted

430 Orbach mechanism that occurs between the $\pm m_j$ degenerate states in the ground state via the highest

431 energy excited m_j state of the Dy^{3+} ion. The calculated energy barrier (Δ) is 31.6 cm^{-1} and the pre-

432 exponential factor (τ_0) of the Arrhenius law is 4.9×10^{-9} s. But linearity is followed only for few

433 points, suggesting that at higher temperature more than one relaxation mechanism is active. Also the

434 distribution of the coefficient values (α) obtained in the fitting by using the generalized Debye model

435 in the Cole–Cole plots, that are in the 0.150–0.002 range, suggest the presence of other relaxation

436 mechanisms such as the QTM, Direct and Raman other than just the Orbach. Thus, the $\ln(\tau)$ vs. $1/T$

437 curve was adjusted taking into account all of the above mechanisms. The best fit was obtained when

438 the spin–lattice relaxation mechanism, Raman and Direct equations are considered, eqn (3).

439
$$\tau^{-1} = CT^n + AH^4T \tag{3}$$

440

441   The obtained parameters from the best fit where $C = 0.011$ s^{-1} $K^{-9.07}$, $n = 9.07$ and $A =$

442 183.29 s^{-1} T^{-4} K^{-1}. For a Kramer ion such as Dy^{3+}, the dependence of τ with T should follow the

443 power law $\tau \propto T^9$ when the relaxation of the magnetization goes through the two phonon relaxation

444 Raman process. Nevertheless, n with values in the interval 1–6 has been claimed to be reasonable

445 when the acoustic phonons are also considered in the spin–lattice relaxation of Raman. Important

446 care has to be taken when fitting the ac data with the different relaxation of the magnetization

447 mechanisms due to over parametrization when using such equations.[33–37]

448   Similar behaviour has been reported for other carboxylate bridged Dy^{3+} complexes and

449   polymeric chains[38–40] and nine coordinate Dy^{3+} compounds with similar coordination geometry as

450   the presented compound.[30,41–43]

451   For compounds S-Tb and S-Sm, no dependence of either magnetic susceptibility components

452   (χ'_M and χ''_M) was observed neither at a 0 dc field nor at higher dc applied fields.

453

454

455

456

4. Conclusion

In this work, eight enantiomerically pure lanthanide coordination compounds have been successfully isolated. The lanthanide compounds consist of a chiral coordination 1D polymer that expands along the a crystallographic axis. The compounds have the [Ln(μ-R/S-MPA)(R/S-MPA)$_2$(phen)]$_n$ formula where R/S-HMPA stands for (R/S)-(±)-α-methoxyphenylacetic acid and Ln = Eu^{3+}, Tb^{3+}, Dy^{3+} and Sm^{3+}. Single crystal X-Ray diffraction measurements were performed for compounds R/S-Eu, R/S-Tb, S-Dy and S-Sm. R/S-Eu, R/S-Tb, R/S-Dy and R/S-Sm coordination compounds have been characterized by means of Powder X-Ray Diffraction and Infrared spectroscopy. Moreover, luminescence studies have been carried out, as all the compounds presented sensitized luminescence associated to the expected f–f transitions. The S-Eu and S-Tb compounds showed rather good luminescence properties with measured Quantum Yields of 0.14 and 0.33 respectively. Also, the luminescence lifetime was measured and from the monoexponential curves, a τ_{obs} of 1.77 ms for R-Eu and of 1.50 ms for R-Tb analogue were extracted. Furthermore, a chiroptical study was performed on these coordination polymers in the solid state. Circular dichroism spectra were recorded and CPL measurements were performed for the most luminescent analogues (R/S-Eu and R/S-Tb). For the europium compounds, mirror image spectra could be obtained where the different f–f transitions can be discerned. On the other hand, for the Tb^{3+} analogue the intensity in the CPL spectra was too low and no reliable conclusions could be extracted from it. Finally, magnetic studies were performed for all the S-enantiomers. Only the S-Dy compound shows slow relaxation of the magnetization under an external magnetic field. Thus, the S-Dy compound displays luminescent, chiral and field-induced SMM properties and can be considered as a multifunctional complex. All luminescence, chirooptical and magnetic measurements were carried out in the solid state since the compounds presented here consist of chiral polymeric chains, which would be disrupted by dissolution into any solvent.

Acknowledgements

References

1   N. Ishikawa, M. Sugita, T. Ishikawa, S. Y. Koshihara and Y. Kaizu, J. Am. Chem. Soc., 2003, 125, 8694.

2   (a) J. Tang and P. Zhang, Lanthanide Single Molecule Magnets, Springer-Verlag, Berlin Heidelberg, 2015; (b) H. L. C. Feltham and S. Brooker, Coord. Chem. Rev., 2014, 276, 1; (c) D. N. Woodruff, R. E. P. Winpenny and R. A. Layfield, Chem. Rev., 2013, 113, 5110; (d) A. Zabalalekuona, J. M. Seco and E. Colacio, Coord. Chem. Rev., 2021, 441, 213984; (e) A. Borah and R. Murugavel, Coord. Chem. Rev., 2022, 453, 214288.

3   (a) The Rare Earth Elements, Fundamentals and Applications, ed. D. A. Atwood, John Wiley& Sons Ltd, 2012; (b) Z. Xia, Z. Xu, M. Chen and Q. Liu, Dalton Trans., 2016, 45, 11214; (c) J.-C. G. Bünzli and C. Piguet, Chem. Soc. Rev., 2005, 34, 1048; (d) J.-C. G. Bünzli, Acc. Chem. Res., 2006, 39, 53; (e) S. Swavey and R. Swavey, Coord. Chem. Rev., 2009, 253, 2627; (f) S. V. Eliseeva and J.-C. G. Bünzli, Chem. Soc. Rev., 2010, 39, 189; (g) E. G. Moore, A. P. S. Samuel and K. N. Raymond, Acc. Chem. Res., 2009, 42, 542; (h) C. P. Montgomery, B. S. Murray, E. J. New, R. Pal and D. Parker, Acc. Chem. Res., 2009, 42, 925; (i) S. J. Butler, M. Delbianco, L. Lamarque, B. K. McMahon, E. R. Neil, R. Pal, D. Parker, J. W. Walton and J. M. Zwier, Dalton Trans., 2015, 44, 4791; (j) J. C. Bünzli, Coord. Chem. Rev., 2015, 293–294, 19; (k) Q. Zhang, W. Ge, X. Zhang and X. Chen, Dalton Trans., 2022, 51, 8714; (l) P. Pradhan, S. Priya, M. Rajendran, K. Singh and S. Vaidyanathan, Dalton Trans., 2022, 51, 715.

4   (a) G. Koeckelberghs, S. Sioncke, T. Verbiest, A. Persoons and C. Samyn, Chem. Mater., 2003, 15, 2870; (b) S. Dang, J.-H. Zhang, Z.-M. Sun and H.-J. Zhang, Chem. Commun., 2012, 48, 11139; (c) E. Peeters, M. P. T. Christiaans, R. A. J. Janssen, H. F. M. Schoo, H. P. J. M. Dekkers and E. W. Meijer, J. Am. Chem. Soc., 1997, 119, 9909; (d) J. P. Leonard, P. Jensen, T. McCabe, J. E. O'Brien, R. D. Peacock, P. E. Kruger and T. Gunnlaugsson, J. Am. Chem. Soc., 2007, 129, 10986; (e) F. Stomeo, C. Lincheneau, J. P. Leonard, J. E. O'Brien, R. D. Peacock, C. P. McCoy and T. Gunnlaugsson, J. Am. Chem. Soc., 2009, 131, 9636.

5   (a) F. Zinna, U. Giovanella and L. Di Bari, Adv. Mater., 2015, 27, 1791; (b) F. Zinna, M. Pasini, F. Galeotti, C. Botta, L. Di Bari and U. Giovanella, Adv. Funct. Mater., 2017, 27, 1603719; (c) F. Zinna, L. Arrico, T. Funaioli, L. di Bari, M. Pasini, C. Botta and U. Giovanella, J. Mater. Chem. C, 2022, 10, 463.

6   (a) S. Shuvaev, E. A. Suturina, K. Mason and D. Parker, Chem. Sci., 2018, 9, 2296; (b) M. Leonzio, A. Melchior, G. Faura, M. Tolazzi, M. Bettinelli, F. Zinna, L. Arrico, L. Di Bari and F.

526 Piccinelli, New J. Chem., 2018, 42, 7931; (c) J. Yuasa, T. Ohno, H. Tsumatori, R. Shiba, H.
527 Kamikubo, M. Kataoka, Y. Hasegawa and T. Kawai, Chem. Commun., 2013, 49, 4604; (d) K. M.
528 Ayers, N. D. Schley and G. Ung, Inorg. Chem., 2020, 59, 7657; (e) J. Gong and X. Zang, Coord.
529 Chem. Rev., 2022, 453, 214329; (f) N. F. M. Mukthar, N. D. Schley and G. Ung, J. Am. Chem.
530 Soc., 2022, 144, 6148; (g) P. Stachelek, L. MacKenzie, D. Parker and R. Pal, Nat. Commun.,
531 2022, 13, 553; (h) A. T. Frawley, R. Pal and D. Parker, Chem. Commun., 2016, 52, 13349.

532 7 (a) M. Górecki, L. Carpita, L. Arrico, F. Zinna and L. Di Bari, Dalton Trans., 2018, 47, 7166; (b)
533 L. E. MacKenzie and R. Pal, Nat. Rev. Chem., 2021, 5, 109–124.

534 8 (a) F. Gendron, S. Di Pietro, L. Abad Galán, F. Riobé, V. Placide, L. Guy, F. Zinna, L. Di Bari, A.
535 Bensalah-Ledoux, Y. Guyot, G. Pilet, F. Pointillard, B. Baguenard, S. Guy, O. Cador, O. Maury
536 and B. Le Guennic, Inorg. Chem. Front., 2021, 8, 914; (b) B. Lefeuvre, C. A. Mattei, J. Flores
537 Gonzalez, F. Gendron, V. Dorcet, F. Riobé, C. Lalli, B. Le Guennic, O. Cador, O. Maury, S. Guy,
538 A. Bensalh-Ledoux, B. Baguenard and F. Pointillard, Chem. – Eur. J., 2021, 27, 7362.

539 9 E. M. Sánchez-Carnerero, A. R. Agarrabeitia, F. Moreno, B. L. Maroto, G. Muller, M. J. Ortiz
540 and S. de la Moya, Chem. – Eur. J., 2015, 21, 13488.

541 10 (a) F. Zinna and L. Di Bari, Chirality, 2015, 27, 1; (b) J. L. Lunkley, D. Shirotani, K. Yamanari, S.
542 Kaizaki and G. Muller, Inorg. Chem., 2011, 50, 12724; (c) F. Zinna, C. Resta, S. Abbate, E.
543 Castiglioni, G. Longhi, P. Mineo and L. Di Bari, Chem. Commun., 2015, 51, 11903.

544 11 (a) M. Cantuel, G. Bernardinelli, G. Muller, J. P. Riehl and C. Piguet, Inorg. Chem., 2004, 43,
545 1840; (b) F. Stomeo, C. Lincheneau, J. P. Leonard, J. E. Obrien, R. D. Peacock, C. P. McCoy and
546 T. Gunnlaugsson, J. Am. Chem. Soc., 2009, 31, 9636.

547 12 (a) O. Mamula, M. Lama, S. G. Telfer, A. Nakamura, R. Kuroda, H. Stoeckli-Evans and R.
548 Scopelitti, Angew. Chem., 2005, 117, 2583; (b) M. Lama, O. Mamula, G. S. Kottas, F. Rizzo, L.
549 De Cola, A. Nakamura, R. Kuroda and H. Stoeckli-Evans, Chem. – Eur. J., 2007, 13, 7358.

550 13 G. Bozoklu, C. Gateau, D. Imbert, J. Pecaut, K. Robeyns, Y. Filinchuk, F. Memon, G. Muller and
551 M. Mazzanti, J. Am. Chem. Soc., 2012, 134, 8372.

552 14 (a) B. Casanovas, F. Zinna, L. Di Bari, M. S. El Fallah, M. Font-Bardía and R. Vicente, Dalton
553 Trans., 2017, 46, 6349; (b) B. Casanovas, S. Speed, M. S. El Fallah, R. Vicente, M. Font-Bardía,
554 F. Zinna and L. Di Bari, Dalton Trans., 2019, 48, 2059.

555 15 (a) K. Miyata, Y. Konno, T. Nakanishi, A. Kobayashi, M. Kato, K. Fushimi and Y. Hasegawa,
556 Angew. Chem., Int. Ed., 2013, 52, 6413; (b) Y. Kuramochi, T. Nakagawa, T. Yokoo, J. Yuasa, T.

557 Kawaia and Y. Hasegawa, Dalton Trans., 2012, 41, 6634; (c) H. Xin, F.-Y. Li, M. Shi, Z.-Q. Bian
558 and C.-H. Huang, J. Am. Chem. Soc., 2003, 125, 7166; (d) A. P. Bassett, S. W. Magennis, P. B.
559 Glover, D. J. Lewis, N. Spencer, S. Parsons, R. M. Williams, L. D. Cola and Z. Pikramenou, J.
560 Am. Chem. Soc., 2004, 126, 9413; (e) X.-P. Yang, R. A. Jones and S.-M. Huang, Coord. Chem.
561 Rev., 2014, 273, 63; (f) M. Tropiano, N. L. Kilah, M. Morten, H. Rahman, J. J. Davis, P. D. Beer
562 and S. Faulkner, J. Am. Chem. Soc., 2011, 133, 11847; (g) J. D. Moore, R. L. Lord, G. A. Cisneros
563 and M. J. Allen, J. Am. Chem. Soc., 2012, 134, 17372; (h) B. Alpha, J.-M. Lehn and G. Mathis,
564 Angew. Chem., Int. Ed. Engl., 1987, 26, 266; (i) C. Bazzicalupi, A. Bencini, A. Bianchi, C. Giorgi,
565 V. Fusi, A. Masotti, B. Valtancoli, A. Roque and F. Pina, Chem. Commun., 2000, 561.

566 16 F. Zinna, T. Bruhn, C. A. Guido, J. Ahrens, M. Bröring, L. Di Bari and G. Pescitelli, Chem. – Eur.
567 J., 2016, 22, 16089.

568 17 G. M. Sheldrick, Acta Crystallogr., Sect. A: Fundam. Crystallogr., 2008, 64, 112.

569 18 G. M. Sheldrick, Acta Crystallogr., Sect. C: Cryst. Struct. Commun., 2015, 71, 3.

570 19 (a) M. Llunell, D. Casanova, J. Cirera, P. Alemany and S. Alvarez, Shape Program., version 2,
571 Universitat de Barcelona, Barcelona, Spain, 2010; (b) P. Alemany, D. Casanova, S. Alvarez, C.
572 Dryzun and D. Avnir, Rev. Comput. Chem., 2017, 30, 2892.

573 20 Luminescence of Lanthanide Ions in Coordination Compounds and Nanomaterials, ed. A. de
574 Bettencourt-Dias, John Wiley & Sons Ltd, 2014.

575 21 K. Binnemans, Coord. Chem. Rev., 2015, 295, 1.

576 22 A. Aebischer, F. Gumy and J.-C. G. Bünzli, Phys. Chem. Chem. Phys., 2009, 11, 1346.

577 23 C. A. Mattei, K. Dhbaibi, B. Lefeuvre, V. Dorcet, G. Argouarch, O. Cador, B. Le Guennic, O.
578 Maury, C. Lalli, S. Guy, A. Bensalah-Ledoux, F. Riobé, B. Baguenard and F. Pointillart, Chirality,
579 2022, 34, 34.

580 24 (a) H.-Y. Wong, W.-S. Lo, K.-H. Yim and G.-L. Law, Chem, 2019, 5, 3058; (b) X.-Z. Li, C.-B. Tian
581 and Q.-F. Sun, Chem. Rev., 2022, 122, 6374; (c) Y. Kitagawa, M. Tsurui and Y. Hasegawa, ACS
582 Omega, 2020, 5, 3786.

583 25 Y. Hasegawa, Y. Miura, Y. Kitagawa, S. Wada, T. Nakanishi, K. Fushimi, T. Seki, H. Ito, T. Iwasa,
584 T. Taketsugu, M. Gon, K. Tanaka, Y. Chujo, S. Hattori, M. Karasawa and K. Ishii, Chem.
585 Commun., 2018, 54, 10695.

586 26 J. Legendziewicz, V. Tsaryuk, V. Zolin, E. Lebedeva, M. Borzechowska and M. Karbowiak, New

587   J. Chem., 2001, 25, 1037.

588 27 A. Arauzo, A. Lazarescu, S. Shova, E. Bartolomé, R. Cases, J. Luzón, J. Bartolomé and C. Turta,
589   Dalton Trans., 2014, 43, 12342.

590 28 M. Andruh, E. Bakalbassis, O. Kahn, J. C. Trombe and P. Porcher, Inorg. Chem., 1993, 32, 1616.

591 29 O. Kahn, Molecular Magnetism, VHC Publishers, Inc., USA, 1993.

592 30 H.-R. Tu, W.-B. Sun, H.-F. Li, P. Chen, Y.-M. Tian, W.-Y. Zhang, Y.-Q. Zhang and P.-F. Yan, Inorg.
593   Chem. Front., 2017, 4, 499.

594 31 Y.-N. Guo, G.-F. Xu, Y. Guo and J. Tang, Dalton Trans., 2011, 40, 9953.

595 32 N. F. Chilton, CC-FIT, program/ https://www.nfchilton.com/software.html, 2014.

596 33 G. Handzlik, M. Magott, M. Arczyński, A. M. Sheveleva, F. Tuna, S. Baranc and D. Pinkowicza,
597   Dalton Trans., 2020, 49, 11942.

598 34 L. Gu and R. Wu, Phys. Rev. B, 2021, 103, 014401.

599 35 K. N. Shrivastava, Phys. Status Solidi B, 1983, 117, 437.

600 36 M. Briganti, F. Santanni, L. Tesi, F. Totti, R. Sessoli and Lunghi, J. Am. Chem. Soc., 2021, 143,
601   13633.

602 37 D. Aravena and E. Ruiz, Dalton Trans., 2020, 49, 9916.

603 38 M. Fang, J.-J. Li, P.-F. Shi, B. Zhao and P. Cheng, Dalton Trans., 2013, 42, 6553.

604 39 J. Tian, B. Li, X. Zhang, X. Li, X. Li and J. Zhang, Dalton Trans., 2013, 42, 8504.

605 40 W.-H. Zhu, X. Xiong, C. Gao, S. Li, Y. Zhang, J. Wang, C. Zhang, A. K. Powell and S. Gao, Dalton
606   Trans., 2017, 46, 14114.

607 41 D. N. Woodruff, R. E. P. Winpenny and R. A. Layfield, Lanthanide Single-Molecule Magnets,
608   Chem. Rev., 2013, 113(7), 5110–5148.

609 42 A. Zabala-Lekuona, J. Cepeda, I. Oyarzabal, A. Rodríguez-Diéguez, J. A. García, J. M. Seco and
610   E. Colacio, CrystEngComm, 2017, 19, 256.

611 43 P. Antal, B. Drahoš, R. Herchel and Z. Trávníček, Dalton Trans., 2016, 45, 15114.

612

613

614

Table 1. Selected bond distances (Å) for R/S-Eu, R/S-Tb, S-Dy and S-Sm

Bond distance (Å)	*R*-Eu	*S*-Eu	*R*-Tb	*S*-Tb	*S*-Dy	*S*-Sm
Ln–O1	2.500(5)	2.478(3)	2.417(2)	2.461(3)	2.456(6)	2.461(2)
LnO2	2.489(5)	2.445(4)	2.4601(18)	2.416(3)	2.464(5)	2.4891(19)
Ln–O4	2.450(6)	2.489(3)	2.4740(18)	2.470(3)	2.395(6)	2.510(2)
Ln–O5	2.476(5)	2.498(3)	2.4674(19)	2.475(3)	2.453(5)	2.4988(18)
Ln–O7	2.396(5)	2.394(3)	2.3688(18)	2.371(2)	2.364(4)	2.4050(19)
Ln–O8	2.388(4)	2.395(2)	2.3639(13)	2.365(2)	2.356(5)	2.4039(19)
Ln–O9	2.539(5)	2.540(3)	2.525(19)	2.521(3)	2.513(5)	2.557(2)
Ln–N1	2.569(5)	2.564(4)	2.545(2)	2.537(3)	2.527(7)	2.583(2)
Ln–N2	2.558(6)	2.567(4)	2.538(2)	2.545(4)	2.523(6)	2.582(2)
Ln⋯Ln (intrachain)	6.048(5)	6.047(4)	6.054(8)	6.036(4)	6.025(4)	6.052(3)
Ln⋯Ln shortest interchain distance	12.298	12.310	12.312	12.326	12.353	12.297

619   **Table 2.** g_{lum} values of the R/S-Eu enantiomeric pair for the $^5D_0 \rightarrow {}^7F_1$ and the $^5D_0 \rightarrow {}^7F_2$ transitions

620

R/S-Eu	$^5D_0 \rightarrow {}^7F_1$	$^5D_0 \rightarrow {}^7F_2$
g_{lum}	± 0.013 (+for *S*-Eu)	± 0.003 (+for *R*-Eu)

621

622

623

624

625

Figure Captions

Scheme 1 R/S-α-Methoxyphenylacetic acid (R/S-HMPA).

Figure. 1. Left, partially labeled plot of compound R-Eu. Phenyl groups and H atoms have been omitted for a better view of the 1D structure. Right, idealized coordination polyhedron (spherical tricapped trigonal prism) compared with the real positions of the coordinating atoms of compound R-Eu.

Scheme 2. Coordination modes of R/S-α-methoxyphenylacetate.

Figure. 2. Compounds R- and S-Eu presented as the mirror image of each other.

Figure. 3. (a) Emission spectra of compound R-Eu (λ_{exc} = 330 nm). Bottom, CPL spectra of S- and R-Eu enantiomers. (b) Emission spectra for complexes R-Tb, R-Dy and R-Sm recorded at λ_{exc} = 330 nm. (c) Lifetimes curves for compounds R-Tb and R-Eu. Solid lines represents mono-exponential fittings.

Figure. 4. Circular dichroism spectra of compounds R/S-Eu, R/S-Tb, R/S-Dy and R/S-Sm measured in the solid state.

Figure. 5. χ_MT temperature dependence measured at an external static field of 0.3 T. Continuous black line corresponds to the fitting of the χ_MT versus T data using eqn (S2)† for compound S-Eu.

Figure. 6. Left, χ''_M vs. frequency plot for compound S-Dy and middle, Cole–Cole plot. Black lines correspond to the fitting with the one component Debye model for both graphics. Right, ln(τ) vs. 1/T plot, dashed line represents the fitting with the Arrhenius law and orange line with eqn (3).
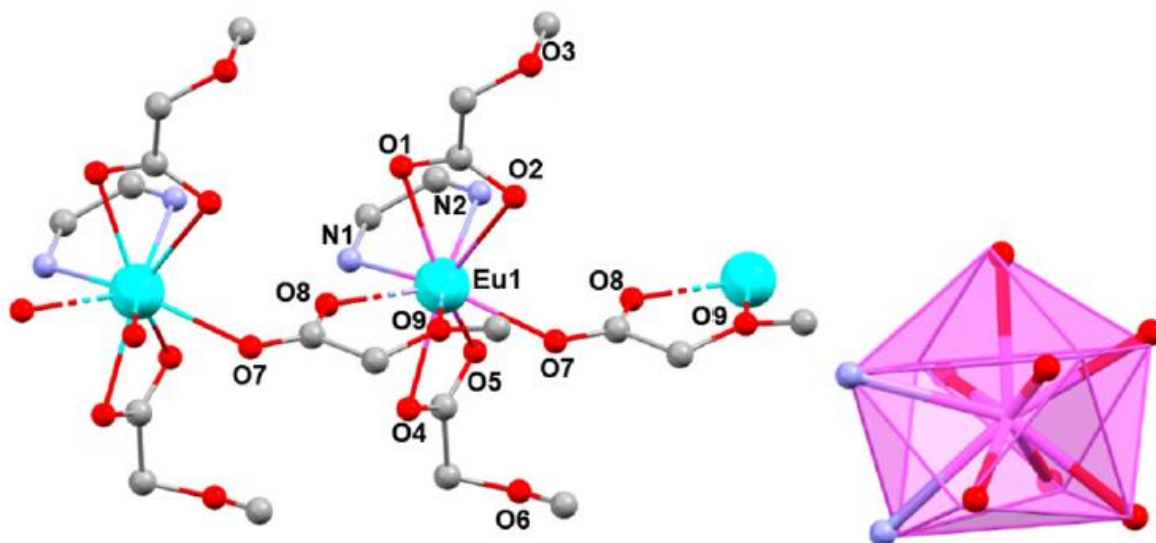
647   **Scheme 1**
648
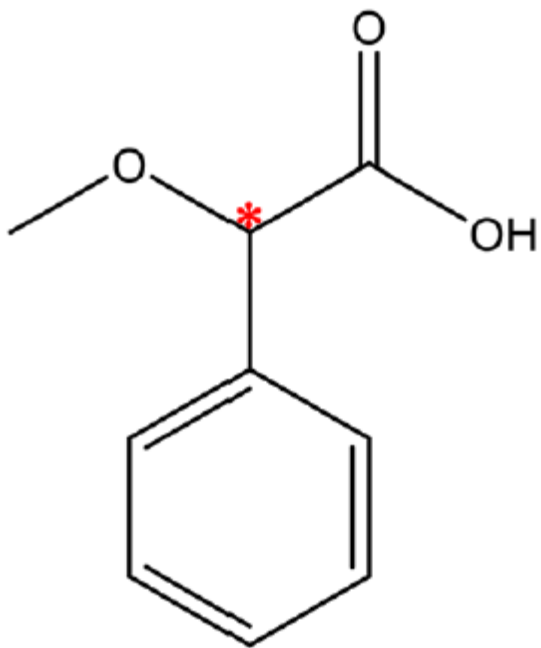
649
650
651
652
653
654
655
656
657
658

Figure 1

Figure 2
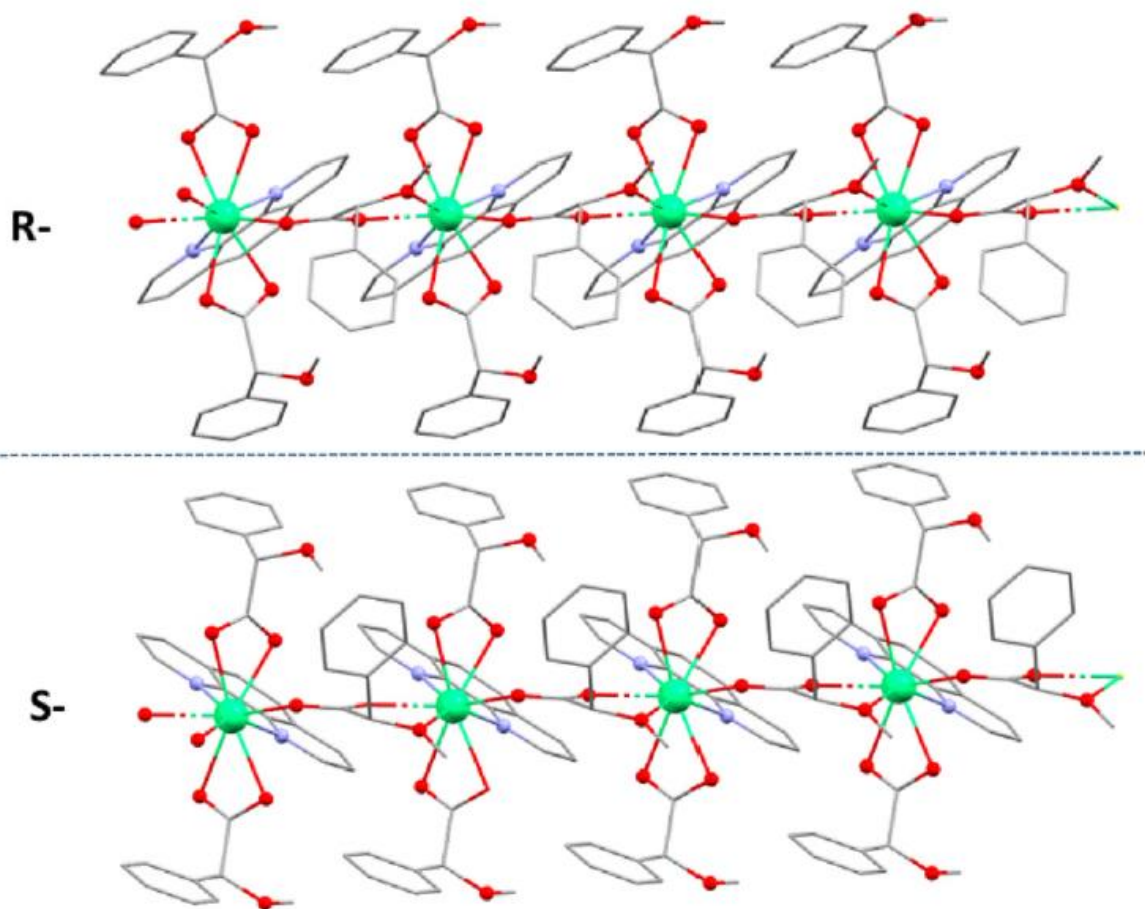
R-
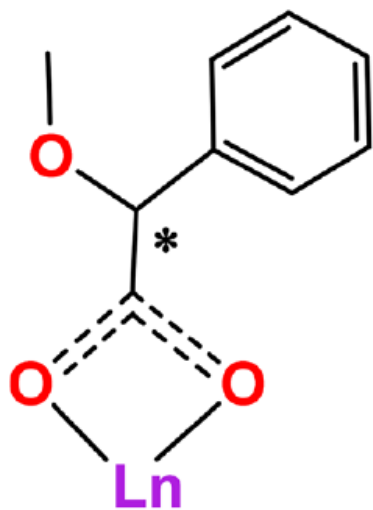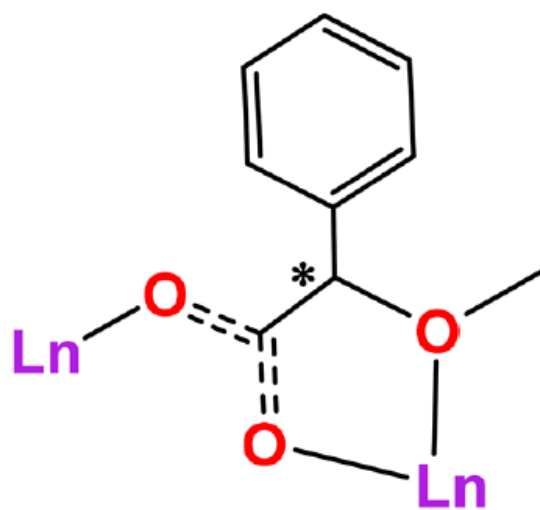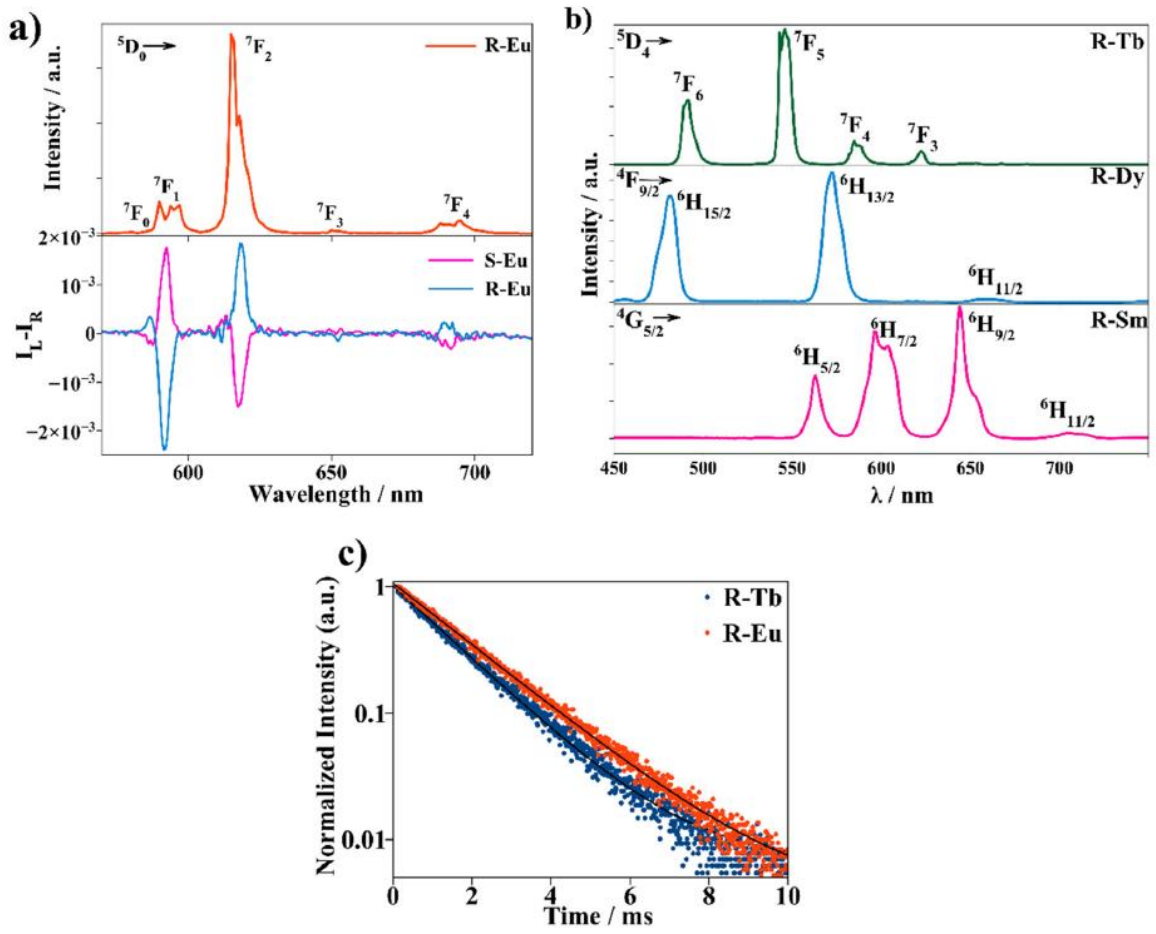
S-

a) Chelating

b) syn-anti, bridging
and chelating

673
674
675
676
677
678
679
680

681 **Figure 3**

682

683
684
685
686
687
688
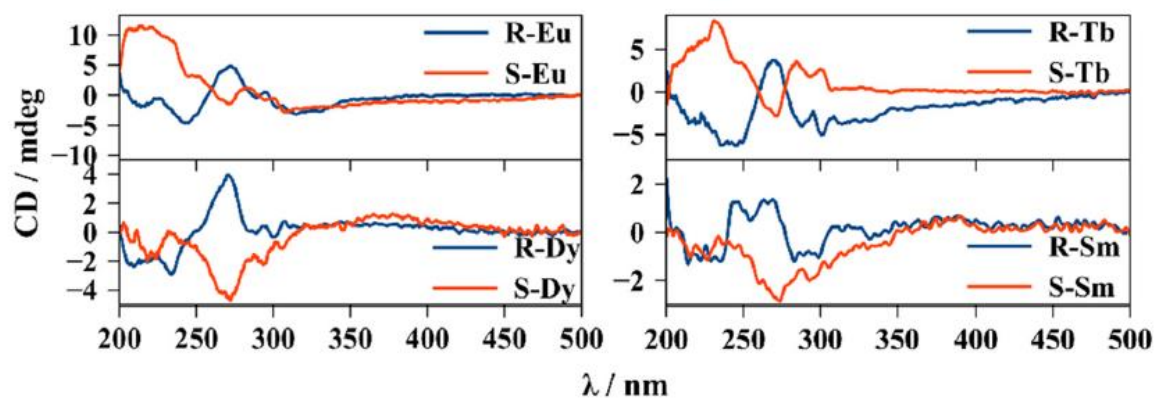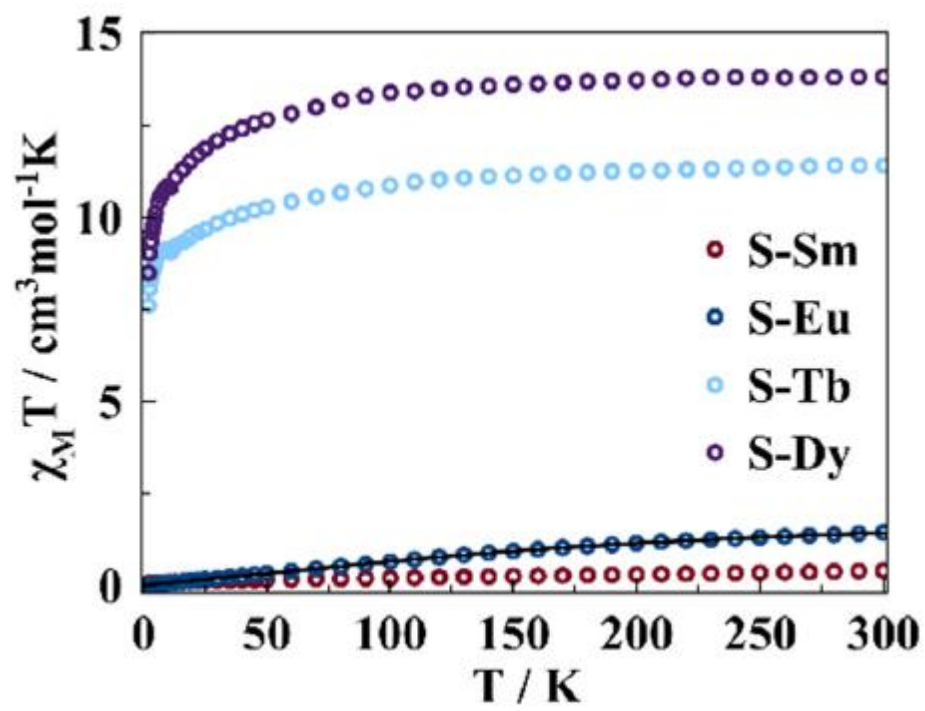689
690
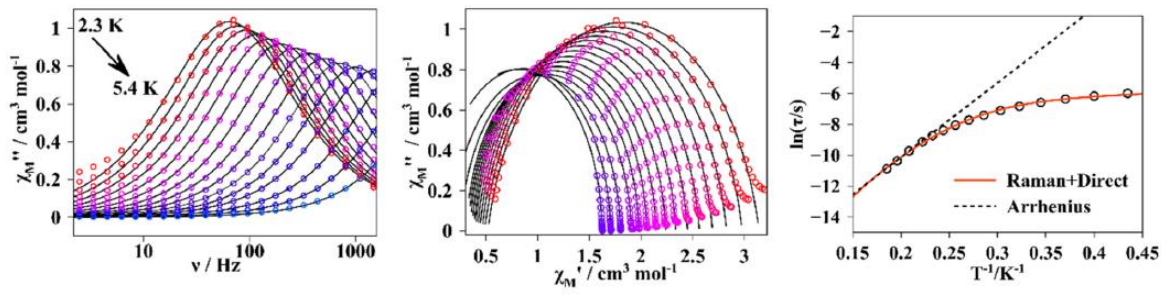
691   **Figure 4**

692

693

694

695 **Figure 5**

696

697

698

699

700

701   **Figure 6**

702

703